

LUT-GEMM: Quantized Matrix Multiplication based on LUTs for Efficient Inference in Large-Scale Generative Language Models

Gunho Park^{*1}, Baeseong Park^{*2}, Minsub Kim², Sungjae Lee², Jeonghoon Kim²
Beomseok Kwon², Se Jung Kwon², Byeongwook Kim², Youngjoo Lee¹, and Dongsoo Lee²

¹ Pohang University of Science and Technology, Pohang, Republic of Korea

² NAVER Cloud, Seongnam, Republic of Korea
dongsoo.lee@navercorp.com

ABSTRACT

The recent advancements in self-supervised learning, combined with the Transformer architecture, have enabled natural language processing (NLP) to achieve remarkably low perplexity. However, powerful NLP models necessitate increasing model size, leading to substantial computational and memory requirements. In this paper, we introduce an efficient inference framework tailored for large-scale generative language models. To reduce the model size, we employ a weight-only quantization strategy while preserving full precision for activations. As a result, we attain sub-4-bit quantization for each weight through non-uniform or uniform quantization techniques. Our proposed kernel, called LUT-GEMM, then accelerates quantized matrix multiplications, offering a flexible balance between compression ratio and accuracy. Unlike earlier matrix multiplication kernels that accommodated weight-only quantization, LUT-GEMM efficiently eliminates the resource-demanding dequantization process for both uniform and non-uniform quantization methods. By reducing the latency of individual GPUs and the overall inference process for large-scale language models, LUT-GEMM provides significant performance improvements in inference. The impact of LUT-GEMM is facilitated by implementing high compression ratios through low-bit quantization and efficient LUT-based operations, which decreases the number of required GPUs. For the OPT-175B model with 3-bit quantization, we show that LUT-GEMM accelerates the latency for generating each token by 2.1 \times compared to OPTQ, which requires costly dequantization. Consequently, LUT-GEMM enables inference of the OPT-175B model on a single GPU without noticeable degradation in accuracy or performance, while the non-quantized OPT-175B model requires a minimum of 8 GPUs.

CCS CONCEPTS

• **Computing methodologies** \rightarrow **Artificial intelligence**; *Parallel computing methodologies*.

KEYWORDS

Neural Network Quantization, Model Compression, Generative Language Model, Transformer, Deep Learning

1 INTRODUCTION

Recent years have observed large-scale language models presenting state-of-the-art performance on various natural language process (NLP) tasks. Such rapid progress in NLP performance has been highly facilitated by the self-supervised learning method. Since

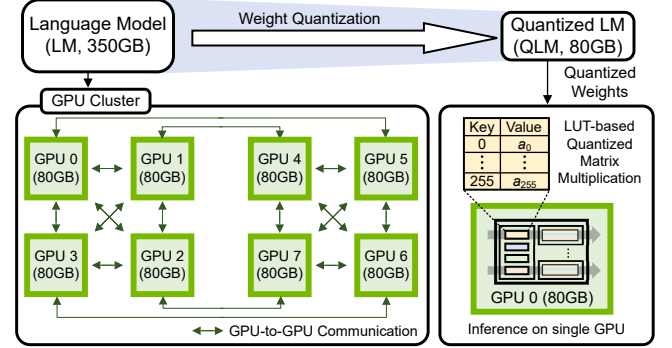


Figure 1: A large language model deployed with 8 GPUs supported by model parallelism, or with 1 GPU only using quantized weights. Assuming 80GB GPU memory size, 8 GPUs are required to serve a 350GB language model unless model compression is implemented.

pre-training dominates the entire training process without an expensive labeling process [3, 8, 15], the size of the training dataset can substantially increase. Combined with efficient sequence-to-sequence model architectures, such as the Transformers [50], the number of model parameters also significantly increases.

Previous studies [6, 23, 26] have reported that LM performance follows a predictable power-law scaling as a function of model size. Accordingly, in recent years, several large-scale generative LMs, including GPT-3 (175B) [6], HyperCLOVA (204B) [27], Gopher (280B) [43], Chinchilla (70B) [23], Megatron Turing NLG (530B) [48], and PaLM (540B) [11], have been proposed to further advance state-of-the-art performance. However, models with billions of parameters cannot be accommodated on a single GPU due to the limited memory size of GPUs, which is sacrificed to enhance memory bandwidth [35, 57]. To address such a concern, researchers have proposed to use model parallelism, which distributes computations over multiple GPUs through GPU-to-GPU communication [38, 47]. As illustrated in Figure 1, model parallelism divides the parameters of a large LM model into several GPUs, allowing information sharing among GPUs during training/inference through dedicated channels.

Model parallelism can be divided into tensor parallelism and pipeline parallelism to improve latency and throughput, respectively. Such parallelism schemes, however, require various communication primitives, such as AllReduce, Reduce, Broadcast, and AllGather, to synchronize partial outputs produced by GPUs [2].

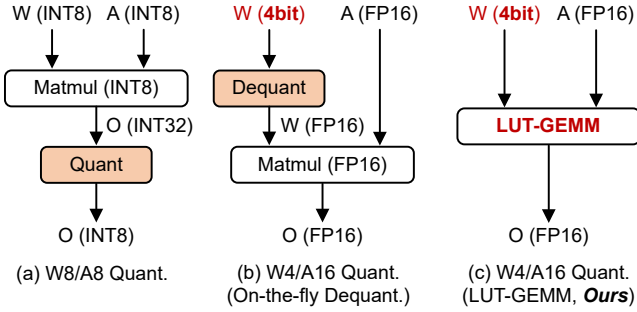


Figure 2: Three matrix multiplication schemes for W8/A8 or W4/A16 (i.e., weight-only) quantization format. Our proposed LUT-GEMM method can accept W4 and A16 without requiring an additional dequantization step.

Even though GPU-specific external communication protocols (e.g., NVLink [30]) can reduce communication latency, an inherent variance of GPU performance (caused by various random factors such as fabrication process variation and operating system conditions) is another performance bottleneck [46]. In addition, since a large matrix is separated into submatrices, each GPU faces tall-and-skinny matrix multiplications with low utilization of resources [4, 25]. As a result, performance gain by model parallelism becomes a sub-linear function of the number of GPUs.

In order to mitigate the challenges related to model parallelism, parameter quantization [10, 33, 54] presents a practical solution for minimizing model size, consequently reducing the number of GPUs required for inference, as described in Figure 1. Among the various quantization schemes, uniform quantization is a favored choice for exploiting integer-based arithmetic units [24, 31, 52, 60]. Nonetheless, uniform quantization is practically limited to 8 bits, and non-linear operations (e.g., softmax and normalization) may yield imprecise results [5, 28]. Moreover, to fully utilize integer arithmetic units, it is essential to implement on-the-fly activation quantization and dequantization, along with an accurate estimation of the activation distribution [14, 56]. Recent research has proposed 4-bit weight-only quantization as an approach for memory compression [18, 58], which involves on-the-fly conversion to full-precision. While this sacrifices the computational benefits of using integer arithmetic, weight-only quantization in large language models (LMs) has provided empirical evidence that the achievable weight compression ratio can be significantly higher for a given target accuracy, as opposed to when both weights and activations are quantized [18, 58]. Various weight-only quantization methods that employ a non-uniform format have also been proposed to improve the compression ratio [25, 29].

In this paper, we introduce a kernel, LUT-GEMM, designed to facilitate quantized matrix multiplications when weights are quantized using either uniform or non-uniform methods while retaining full-precision activations. As shown in Figure 2, LUT-GEMM effectively addresses two issues prevalent in previous quantization approaches: 1) the inevitable degradation of accuracy due to quantized activations and 2) the need for additional dequantization implementation. LUT-GEMM inherently accommodates quantized weights and full-precision activations, enabling the acceleration of

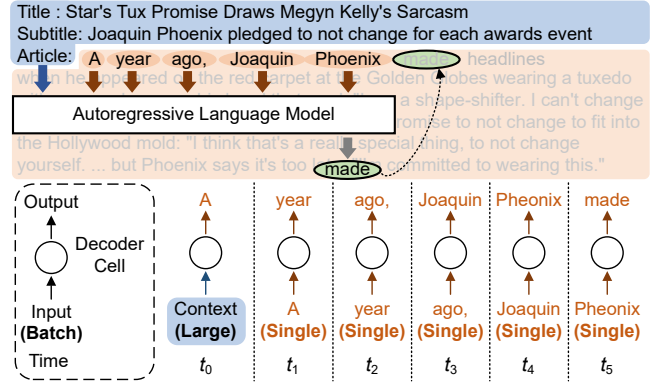


Figure 3: An illustration of the generative language model. Given an input context, a single token is generated in an autoregressive manner. The entire generation procedure can be categorized into the summarization stage (along with a large batch size using an input context) and the generation stage executing single-batch operations using the previously generated token.

the inference process while preserving the desired level of precision. Specifically, LUT-GEMM employs the binary-coding quantization (BCQ) format [45] to capitalize on simple arithmetic operations. It is worth noting that BCQ was initially proposed to support non-uniform quantization, which relies on customized hardware for bit-level operations. In this paper, we demonstrate that prior uniform quantization can be reformulated in the form of BCQ, allowing LUT-GEMM to support both non-uniform and uniform quantization formats. Consequently, LUT-GEMM is capable of executing a wide range of weight-only quantization schemes for matrix multiplications, achieving low inference latency and eliminating the need for activation quantization.

Our major contributions in this work include the following:

- We verify that BCQ is capable of representing both uniform and non-uniform weight quantization.
- We show that, for the BCQ format, LUT-GEMM can provide a wide search space of trade-offs between compression ratio and latency (based on GPU-specific efficient hardware utilization method to implement various BCQ configurations).
- For large LMs, we demonstrate that LUT-GEMM can considerably accelerate matrix multiplications with small quantization bits while power consumption is saved a lot by reducing the number of GPUs. Consequently, LUT-GEMM leads to low energy consumption.
- Assuming a 3-bit BCQ format for weights of OPT-175B, to be served by a single GPU, our experimental results show that LUT-GEMM can accelerate the latency for generating each token by 2.1× compared to the OPTQ [18] results.

2 BACKGROUND

2.1 Generative Language Models

Large-scale generative LMs, such as GPT-3, are autoregressive models that predict future tokens using the previous tokens in a feed-forward fashion. For example, as shown in Figure 3, if an input

context is provided (as in in-context learning [6]), the next token can be predicted by using the previously generated tokens.

The Transformer’s architecture, featuring self-attention mechanism and parallelized training algorithm [50], is widely used in large-scale generative LMs. The number of parameters in generative LMs is increasing thanks to self-supervised learning and the scaling-law [6, 26], which provides predictable performance on the cross-entropy loss as the model size increases. Surprising qualitative evaluation results (e.g., human-like writing) of extreme-scale LMs also fueled the competition in model size [27, 43].

2.2 GPU-Accelerated Generative LMs

For large LMs, the processing time of matrix multiplications dominates the entire inference latency because of higher time complexity compared to activation functions, normalization layers, and so on [14]. To validate such a claim, Figure 4 shows the latency breakdown of various large-scale generative LMs (OPT 6.7B, 13B, 30B, 66B, and 175B) with a different number of input tokens. The OPT models follow the Transformer architecture [50], consisting of identical layers. Let m represent the hidden size (d_{model}). Each layer contains multi-head attention and a feed-forward network, including four primary linear computations with higher time complexity (compared to other non-linear operations). These involve multiplying an $(m \times 1)$ activation matrix with the following four matrices: 1) a $(3m \times m)$ matrix for attention’s key, query, and value, 2) an $(m \times m)$ matrix for attention output, 3) a $(4m \times m)$ matrix for the first feed-forward sub-layer, and 4) an $(m \times 4m)$ matrix for the second sub-layer. All layers have identical structures, and matrix multiplications dominate the entire inference latency [12]. Figure 4 is obtained by A100 (80GB) and FasterTransformer, inference framework of Nvidia¹. Matrix multiplications account for at least 75% of the processing time for various LM sizes and input token lengths (note that due to the limited memory capacity of a single GPU, large LMs may need multiple GPUs, resulting in increased communication latency). GPUs are commonly adopted to accelerate inference as GPUs embed lots of arithmetic units and support multiple threads, critical for speeding up matrix multiplications [35, 38]. However, extracting high performance from GPUs depends on arithmetic intensity, and therefore, the batch size should be large enough to ensure a high reuse ratio from main memory [32].

Tensor Parallelism. For highly parallel computing systems, high memory bandwidth is essential to feed lots of arithmetic units so as to maintain high resource utilization. The main memory system of GPUs, hence, is inclined to focus on high bandwidth instead of large capacity. Correspondingly, even though new innovative memory architectures (e.g., HBM [44]) are proposed, the maximum memory capacity for a single GPU is still limited up to a few tens of gigabytes [30]. Such limited GPU’s memory capacity derived various parallelism ideas to partition a large-scale LM over multiple GPUs [38, 47]. Tensor parallelism can split matrix multiplications over multiple GPUs so as to generate smaller sub-tasks executed simultaneously. Note that such parallelism induces additional synchronization and GPU-to-GPU communication overhead.

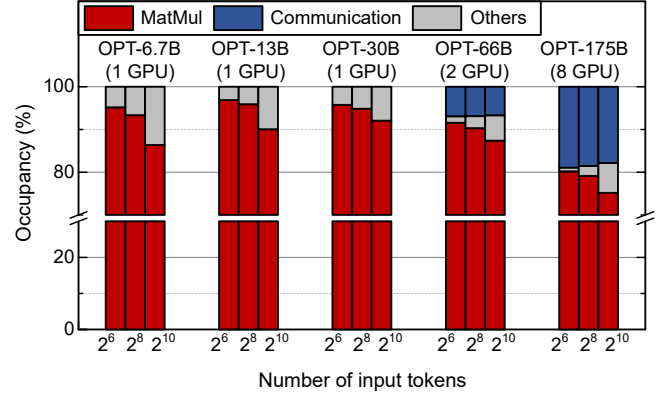


Figure 4: Latency breakdown of various OPT models. The overall performance is dominated by MatMul and communication operations. Experiments are conducted with A100 80GB and FasterTransformer (v4.0) framework.

Memory-bound Text Generation. In the summarization phase depicted in Figure 3, there is a significant demand for computational resources and a high likelihood of weight reuse. Therefore, employing tensor parallelism across multiple GPUs may effectively improve inference performance. Conversely, the generation phase in Figure 3 presents a memory-bound workload due to its autoregressive nature. Consequently, increasing the number of GPUs in conjunction with tensor parallelism may not be a cost-effective solution, particularly when considering the communication overhead between GPUs. As generation phases become increasingly important for services like ChatGPT [39], addressing the issue of limited memory bandwidth becomes crucial. Regrettably, augmenting memory bandwidth through hardware advancements often encounters physical limitations and is associated with excessive power consumption [42, 61]. Therefore, it is imperative to focus research efforts on model compression techniques that can alleviate memory bottlenecks.

2.3 Quantization Methods and Limitations

Various research efforts have been made to enhance the serviceability of large and heavy deep neural networks by improving their latency and throughput. These efforts include quantization [12, 24, 37, 45, 54], pruning [17, 19, 21, 62], knowledge distillation [22, 41], and low-rank approximation [7, 16, 36]. Among these, quantization is the most extensively researched field, which involves using faster and more efficient computing units and reducing memory usage. Uniform quantization using an INT8 operator is particularly well-studied among the various quantization formats and is currently being actively applied in LLMs [14, 53, 56].

INT8 arithmetic units, commonly found in contemporary computing systems, offer reduced latency (thanks to their low area and power requirements) and decreased memory usage of up to 50% compared to FP16. Thus, present NVIDIA GPUs employ Tensor cores that support INT8 operations to accelerate computations [32]. However, the utilization of INT8 mandates the quantization of activations, which can pose a significant challenge in achieving compressed and accelerated models employing INT8 units. For

¹<https://github.com/NVIDIA/FasterTransformer>

instance, when scaling factors are determined offline, activation quantization may lead to a considerable reduction in model accuracy as outliers are approximated. To circumvent this decline in accuracy, token-based dynamic quantization has emerged as a crucial technique for quantizing LLMs [14, 56]. The LLM.int8() method [14] addresses the systematic appearance of outliers in LLMs by proposing a decomposition method that conducts most of the computation in INT8 and dequantizes a limited number of outliers to FP16, resulting in only a marginal latency decrease in LLMs.

SmoothQuant [53] takes an advanced approach by mathematically transferring the variance of activations, which are challenging to quantize due to the presence of outliers, to weights which are relatively easier to quantize. This technique enables efficient computation of LLMs using INT8 arithmetic units (i.e., W8A8), even when employing static quantization of activations. According to SmoothQuant’s results, LLMs can be accelerated up to 1.5× with a 2× reduction in GPU usage when outliers systematically emerge. However, it should be noted that to apply SmoothQuant in novel LLMs, it is necessary to empirically observe and validate the occurrence of outliers before applying the migration technique.

On the other hand, as previously discussed, the auto-regressive characteristic of the token generation process limits the maximum throughput of hardware, even with INT8 precision. Therefore, services such as chatGPT [39], which require the generation of a large number of tokens, may not experience significant performance improvements through the adoption of INT8 precision.

Recent studies have focused on the inefficiency of the generation step and, in response, proposed the utilization of the W4A16 format [18, 58], which compresses model weights into 4-bit integers without quantizing the activations. Given that current computing systems cannot accelerate the W4A16 format, OPTQ [18] solves such an issue by first dequantizing the weights to an FP16 format on-the-fly and then performing the matrix multiplication operation. By leveraging the memory-bounded characteristics of the generation step, this approach can reduce the number of GPUs and improve generation latency, despite the dequantization overheads.

2.4 Binary-Coding Quantization

In this paper, we present the application of binary-coding quantization (BCQ), a versatile non-uniform quantization scheme that encompasses uniform quantization, as we discuss in the subsequent section. BCQ was first introduced in [45] as a compelling alternative to conventional uniform quantization methods. When a weight vector \mathbf{w} (of size n) is quantized by BCQ and q is the number of quantization bits, \mathbf{w} is approximated to be $\sum_{i=1}^q \alpha_i \mathbf{b}_i$ where $\alpha_i \in \mathbb{R}^+$ is a scaling factor and $\mathbf{b}_i \in \{-1, +1\}^n$ is a binary vector. Note that a scaling factor α can be shared by many weights (n can be any number) such that larger n value results in a relatively smaller memory footprint for scaling factors. The quantization process broadly involves finding scaling factors and binary vectors to minimize the quantization error as follows:

$$\arg \min_{\alpha, \mathbf{b}} \left\| \mathbf{w} - \sum_{i=1}^q \alpha_i \mathbf{b}_i \right\|^2, \quad (1)$$

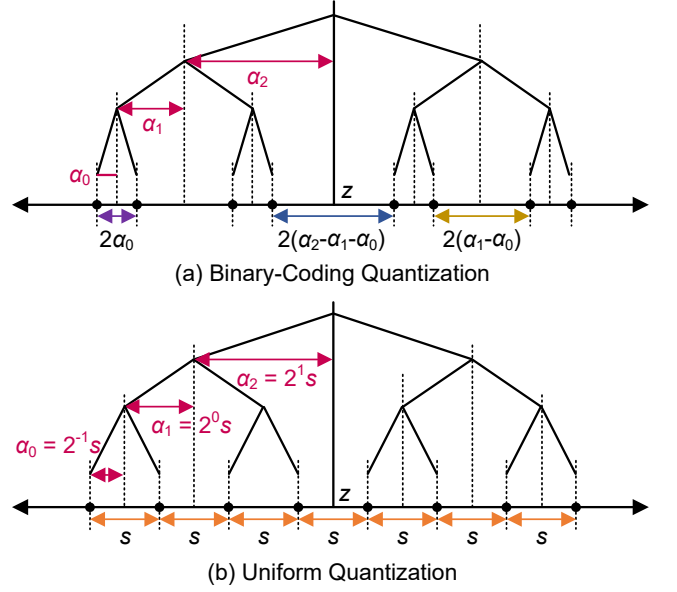


Figure 5: Extension of binary-coding quantization to support both non-uniform and uniform quantization formats, achieved by including a bias term.

which does not have analytical solutions except when $q = 1$. Thus, scaling factors and binary vectors are obtained by iterative search methods [20, 54] or by quantization-aware training [12]. Recently, Kwon et al. [29] proposed AlphaTuning, a method that combines parameter-efficient adaptation and BCQ schemes, demonstrating that various generative LMs can be fine-tuned with downstream dataset while achieving extremely low-bit quantization, even as low as 1 or 2 bits.

3 DESIGN METHODOLOGY OF LUT-GEMM

LUT-GEMM is devised to develop high-performance, low-energy inference systems for LLMs. To achieve this objective, LUT-GEMM incorporates several innovative approaches. Firstly, we expand conventional BCQ methods by adding a bias term, which significantly enhances the representational capacity. This simple addition enables the representation of both non-uniform and uniform quantization methods within the extended BCQ format, allowing us to leverage various quantization methods, depending on the specific LLM requirements. Secondly, We further refine the implementation details of the binary-coding quantization scheme, enabling a trade-off between compression ratio and quantization error to better exploit the characteristics of LLMs. Lastly, since most non-uniform quantization methods typically involve complex operations with low parallelism and may lack hardware support, we design LUT-GEMM to efficiently accommodate BCQ formats. Our proposed kernel, LUT-GEMM, directly utilizes BCQ formats, eliminating the need for additional overhead, such as dequantization. As a result, LUT-GEMM demonstrates reduced latency and/or a decreased number of GPUs required for LLM inference, while inherently accommodating various weight-only quantization methods.

3.1 Extension of Binary-Coding Quantization

Asymmetric Binary-Coding Quantization. Conventional BCQ methods are basically limited to exhibiting symmetric quantization shape with respect to the zero point. Another constraint of BCQ methods stems from their inability to represent the value of zero due to the symmetric quantization properties. To enhance the representational capacity of BCQ, we extend the conventional BCQ method by including a bias term z as follows:

$$\hat{w} = \sum_{i=0}^{q-1} (\alpha_i \cdot \mathbf{b}_i) + z, \quad \mathbf{b}_i \in [-1, +1] \quad (2)$$

, where a weight matrix is divided into binary vector \mathbf{b}_i with associated scaling factor vectors α_i . As a result, the modified BCQ format, along with the inclusion of the bias term, can represent asymmetry quantization centered around z , as illustrated in Figure 5(a).

Uniform Quantization. We show that the introduction of the bias term in the BCQ format enables the representation of uniform quantization within the extended BCQ format by carefully adjusting the scaling factors and bias term (Figure 5(b)). Let us illustrate the details of how asymmetric uniform quantization can be converted into symmetric BCQ with a bias term. A q -bit uniformly quantized weight \hat{w} with a scaling factor s can be expressed (prior to conversion) as follows:

$$\hat{w} = s \sum_{i=0}^{q-1} 2^i \hat{\mathbf{b}}_i + \hat{z}, \quad \hat{\mathbf{b}}_i \in [0, 1]. \quad (3)$$

Then, \hat{w} can be rewritten as:

$$\begin{aligned} \hat{w} &= \frac{1}{2}s \sum_{i=0}^{q-1} 2^i \cdot 2\hat{\mathbf{b}}_i + \hat{z}, \\ &= \sum_{i=0}^{q-1} \frac{1}{2}s \cdot 2^i (2\hat{\mathbf{b}}_i - 1) + \sum_{i=0}^{q-1} \frac{1}{2}s \cdot 2^i + \hat{z}, \end{aligned} \quad (4)$$

Given that a binary weight b in the BCQ format can be defined as $b = 2\hat{b} - 1$, we obtain

$$\hat{w} = \sum_{i=0}^{q-1} (2^{i-1}s \cdot \mathbf{b}_i) + \left(\sum_{i=0}^{q-1} \frac{1}{2}s \cdot 2^i + \hat{z} \right), \quad (5)$$

which can be interpreted as a special case of BCQ, where $\alpha_i = 2^{i-1}s$ and $z = \sum_{i=0}^{q-1} \frac{1}{2}s \cdot 2^i + \hat{z}$ in Equation 2. In Figure 5, we can see that for q -bit quantization, the uniform quantization method employs a single scaling factor, while the non-uniform quantization technique calls for the use of q distinct scaling factors. Consequently, due to the incorporation of the extended binary-coding quantization format, our proposed LUT-based matrix multiplication scheme is applicable to both uniform quantization and binary-coding-based non-uniform quantization methods.

3.2 Group-wise α Assignment

In practice, conventional BCQ methods assume that a scaling factor is assigned to each row of a weight matrix (or even to the entire matrix) so as to support vector instructions of CPUs or GPUs [45, 54]. As large-scale LMs introduce deeper and wider model

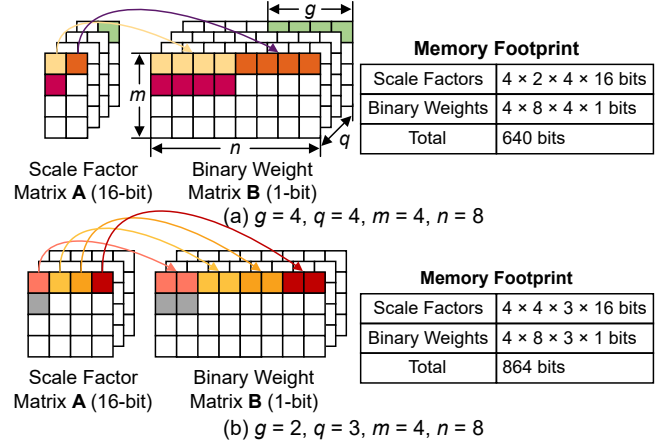


Figure 6: Group-wise BCQ example with two different (g, q) configurations to quantize an (4×8) matrix. Assuming a scaling factor of 16 bits, smaller q can yield a larger memory footprint if g is also small.

structures along with ever-increasing parameter size [43, 47], however, we argue that such conventional row-wise BCQ format encounters various challenges. Suppose that a relatively small hidden size (e.g., $d_{\text{model}} = 1024$ for OPT 350M) is selected along with small weight matrices correspondingly, row-wise assignment of scaling factors might be reasonable to obtain low quantization error. On the other hand, if the hidden size increases rapidly (e.g., $d_{\text{model}} = 12288$ for GPT-3 175B) according to the advent of large-scale LMs, it would be more difficult to compute a proper scaling factor shared by a larger number of weights. In order to enable low-bit quantization schemes, it would be necessary to investigate different ways of assigning scaling factors as long as a new assignment can be backed by practical implementation.

As an alternative to row-wise quantization, we propose group-wise quantization in which a scaling factor can be shared by an arbitrary number of weights. Our proposed new BCQ format introduces a new hyper-parameter g as a group size that represents the number of weights to be shared by a scaling factor. In this paper, g is a fixed number with a range of 32 to the column width of a matrix (equivalent to row-wise quantization). Since g is a constant number, the hidden size does not affect our group-wise BCQ formats.

Impact on Compression Ratio. Let q be the number of quantization bits. For a given q , a smaller group size g can lower quantization error at the expense of an increased memory footprint for scaling factors. Then, the target quantization error serves as a constraint for determining a compromise between q and g , thus resulting in a range of achievable compression ratios. In other words, due to the introduction of g , we can control the amount of scaling factors and binary vectors as a trade-off process. Note that the memory footprint of conventional row-wise quantization techniques is dominated by the size of binary vectors because the size of scaling factors can usually be ignored if the column width of a matrix is large enough. Compared to the conventional scheme, our proposed group-wise BCQ provides a new wide search space for

Table 1: Example of a lookup table to store pre-computed values with a sub-vector of \mathbf{x} when $\mu=3$.

Binary Patterns	Key	Value
$\{-1, -1, -1\}$	0 (b'000)	$-x_1 - x_2 - x_3$
$\{-1, -1, +1\}$	1 (b'001)	$-x_1 - x_2 + x_3$
$\{-1, +1, -1\}$	2 (b'010)	$-x_1 + x_2 - x_3$
$\{-1, +1, +1\}$	3 (b'011)	$-x_1 + x_2 + x_3$
$\{+1, -1, -1\}$	4 (b'100)	$+x_1 - x_2 - x_3$
$\{+1, -1, +1\}$	5 (b'101)	$+x_1 - x_2 + x_3$
$\{+1, +1, -1\}$	6 (b'110)	$+x_1 + x_2 - x_3$
$\{+1, +1, +1\}$	7 (b'111)	$+x_1 + x_2 + x_3$

quantization formats to meet a target compression ratio. Figure 6 shows an example with two (g, q) configurations to quantize an (4×8) matrix. Indeed, even if the number of quantization bits is smaller, the memory footprint can be large when the group size g is small (i.e., more scaling factors are employed).

3.3 LUT based Quantized Matrix Multiplication

Our quantization scheme, which utilizes BCQ format for weight quantization while maintaining full precision for activations, leads to duplicate and redundant partial computations in naive matrix multiplications. To illustrate, assume that a binary matrix $\mathbf{B} \in \{-1, +1\}^{4 \times 4}$ and an activation vector $\mathbf{x} \in \mathbb{R}^4$ are given as

$$\mathbf{B} = \begin{bmatrix} +1 & -1 & -1 & +1 \\ +1 & -1 & +1 & -1 \\ +1 & -1 & -1 & -1 \\ -1 & +1 & -1 & +1 \end{bmatrix}, \quad \mathbf{x}^\top = \begin{bmatrix} 1.2 \\ -0.7 \\ 0.3 \\ 0.6 \end{bmatrix}. \quad (6)$$

Then, computing $\mathbf{B}\mathbf{x}^\top$ (that is to be multiplied by scaling factors) would repeat $(1.2 - (-0.7))$ three times and $(-0.3 + 0.6)$ two times. Such redundant computations are caused by digitized elements of \mathbf{B} , and thus, we expect more duplicated computations as the size of matrices increases according to the growth of model size. Moreover, loading each element of \mathbf{B} requires bit-level memory accesses that can be slow for commercial CPUs and GPUs.

To avoid bit-level memory accesses and perform $\mathbf{B}\mathbf{x}^\top$ efficiently, we can pre-compute all possible combinations of full-precision activations and binary patterns. Note that a lookup table (LUT) has been widely used to save processing time when numerous computations yield outputs within a restricted set [13, 34, 55]. LUT-based computation is justified especially when retrieving a value from a LUT is much faster than carrying out the original calculations. BCQ format (without quantizing activations that require heavy modifications in training codes and model structure [24, 52]) is also useful to be implemented by LUT-based approaches. For example, with every 3 elements $\{x_1, x_2, x_3\}$ in \mathbf{x} , we can pre-compute $8 (=2^3)$ possible values as shown in Table 1 and store those values in a LUT. Let μ be the length of a sub-vector of \mathbf{x} to construct a LUT (hence, μ is 3 in Table 1). Once 2^μ values of a LUT are generated by using a sub-vector of \mathbf{x} , arithmetic operations to obtain partial dot products (of $\mathbf{B}\mathbf{x}^\top$) are replaced with LUT retrieval operations while a key is given by concatenating μ binary elements of \mathbf{B} . To complete $\mathbf{B}\mathbf{x}^\top$ computation, as the final step, those partial products are summed and then multiplied by scaling factors. When the row dimension of \mathbf{B} is enlarged (as generative LMs get

larger), the utilization of a LUT increases due to more occurrences of redundant computations.

Let us briefly explain how to optimize μ , which is also discussed in [25]. If μ increases, LUT construction cost increases as well by 2^μ . Such increased μ , however, can enhance computational parallelism because we can replace the μ number of FP16 additions with one LUT retrieval operation. Thus, as reported in [25], there exists an optimal μ to maximize the speed-up. Note that optimizing μ also needs to consider aligned memory accesses. In our work, $\mu = 8$ is used as a practical choice.

3.4 Proposed LUT-GEMM

In addition to the LUT-based scheme (eliminating redundant computations and bit-level memory accesses), our proposed LUT-GEMM needs to achieve high performance with group-wise quantization in order to enhance accuracy for a given q . Our strategy for optimizing single-batch operations on GPUs is as follows:

- To improve parallelism, we create as many threads as possible while each thread is allowed to perform independent LUT accesses.
- Binary weights accessed by a thread can share a common scaling factor such that operations related to scaling factors do not degrade the performance of a thread.
- If we allocate too small resources to a thread, then LUT utilization can be low, and synchronization overhead can increase. As such, we need to optimize thread configurations empirically.

For the sake of simplicity, we formulate the proposed group-wise quantized matrix multiplication as $\mathbf{y} = \sum_{i=1}^q (\mathbf{A}_i \circ (\mathbf{B}_i \cdot \mathbf{x}))$, where \mathbf{A} is an $(m \times n)$ FP16 scaling matrix, \mathbf{B} is an $(m \times n)$ FP16 binary matrix, \mathbf{x} is an FP16 input vector of size n , and the operator \circ indicates element-wise multiplication. Note that in real situations, the memory footprint of \mathbf{A} is reduced by g since every g weights share a scaling factor.

Overall Architecture. For LUT-GEMM, we assign l LUTs to a thread block (TB) of GPU. Then, the size of submatrix of \mathbf{A} and \mathbf{B} allocated to each TB becomes $(t_h \times t_w)$ when $t_w = l \times \mu$. Small t_h can increase the number of available threads while large t_h enhances LUT utilization inside a TB. Thus, t_h is empirically determined (2048 is a practical number for large-scale LMs). Note that the amount of resources allocated to each TB is small enough such that multiple TBs can share a scaling factor as long as g is larger than $l \times \mu$. The overall LUT-GEMM implementation scheme on GPUs is presented in Figure 7 when we assume $\mu = 8$, $l = 4$, $t_w = 32$, $t_h = 4$, $q = 1$, and $g = 32$. For $q > 1$, the entire process of Figure 7 can be iterated q times while intermediate results are accumulated.

Detailed Implementation. Each TB first conducts pre-computation using partial \mathbf{x} values assigned in order to fill up the l number of LUTs. Then l LUTs can be shared by all threads inside a TB (so as to mitigate costly global memory accesses) and multiple rows of a submatrix of \mathbf{B} can be processed by multiple threads (so as to improve throughput). When threads finish retrieving and summing LUT values, scaling factors are fetched (only once for each

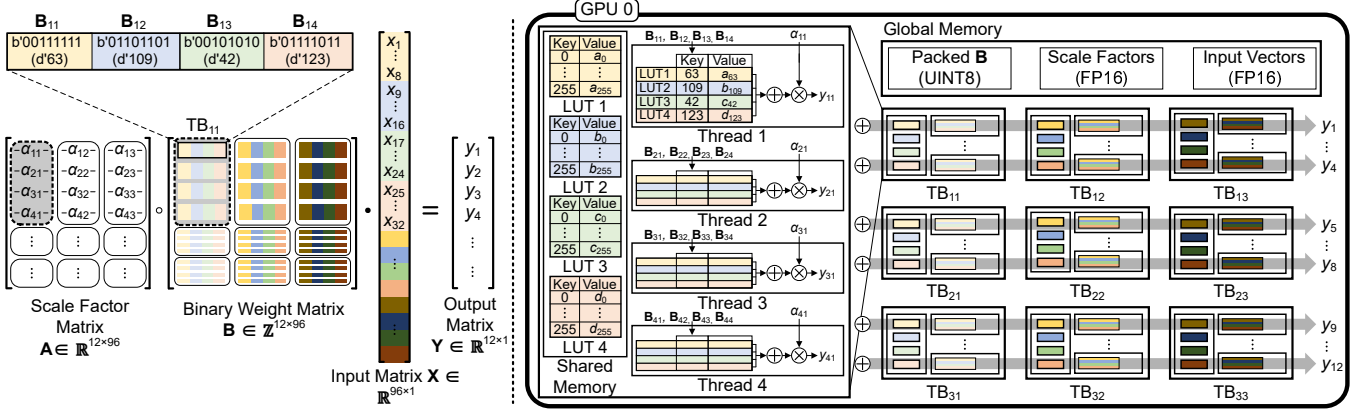


Figure 7: The overview of LUT-GEMM implementation on GPUs. In this example, we assume $m = 12$, $n = 96$, $\mu = 8$, $t_h = 4$, $l = 4$, $t_w = 32$, $q = 1$, and $g = 32$. “ \circ ” denotes element-wise multiplication and “ \cdot ” indicates a tensor product.

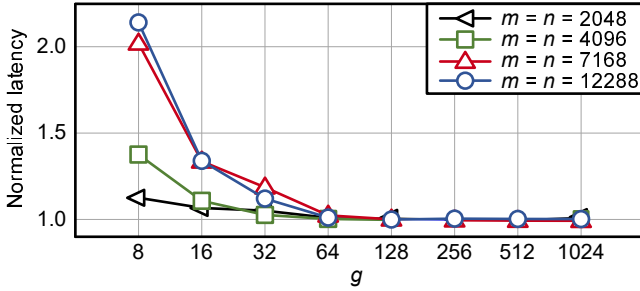


Figure 8: Normalized matrix multiplication latency when a $(m \times n)$ weight matrix is quantized by $(q=3)$ bits with different g values.

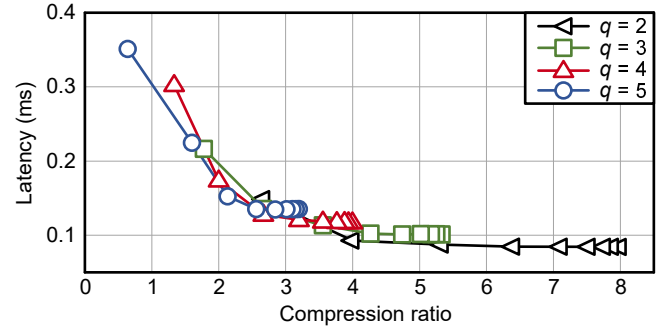


Figure 9: Relationship between latency and compression ratio when LUT-GEMM performs quantized matrix multiplications with $m = n = 12288$ and various (q, g) pairs.

thread) and multiplied to produce partial outputs. Finally, $\frac{n}{l \times \mu}$ partial outputs are accumulated across TBs (through atomicAdd operations, as illustrated in Figure 7) to generate the final outputs. LUTs are stored in shared memory inside GPU and the shared memory presents high bandwidth (e.g., 19TB/s for A100). Thus, high memory accesses for LUTs (while multiple FLOPs can be replaced with one LUT access) enable fast matrix computations. As for the memory size of LUTs, only 1KB is required for every 8 hidden dimensions and the shared memory size is more than a few megabytes (e.g., 20MB for A100 with 192KB per SM and 108 SMs available). Thus, the whole LUTs can be safely stored in shared memory. To illustrate, the hidden dimension can be up to 324,000 for A100 while 12,288 is the hidden dimension for GPT-3 175B.

To examine the latency variance of LUT-GEMM on group size g , we perform matrix multiplications (using an $(m \times n)$ matrix and an $(n \times 1)$ matrix) when g values vary. In Figure 8, for each $m (= n)$ selection, matrix multiplication latency of different g is compared with that of row-wise (i.e., $g = n$) BCQ format. Interestingly, when $g > 32$, group-wise LUT-GEMM is as fast as row-wise LUT-GEMM regardless of m in Fig 8. In other words, a reasonably large g (such as 128 and 256) can result in fast LUT-GEMM while accuracy improvement by group-wise is substantial.

To gain insights into the underlying mechanisms in Figure 8, we analyze the memory footprint of LUT-GEMM because single-batch operations are primarily memory-bound and latency is proportional to the memory footprint. Let S_b and S_α represent the space complexity of binary weights and scaling factors, respectively. Then the overall space complexity S can be described as

$$S = S_b + S_\alpha = O\left(1 \cdot m \cdot n \cdot q + 16 \cdot m \cdot \frac{n}{g} \cdot q\right) \quad (7)$$

$$= O\left(m \cdot n \cdot q \left(1 + \frac{16}{g}\right)\right).$$

As a consequence, if $g \gg 16$, S can be independent of g and approximated to be $O(m \cdot n \cdot q)$. To verify our claim that latency of LUT-GEMM is proportional to memory footprint (when running single-batch operations), we explore various (q, g) pairs and compression ratios correspondingly and measure matrix multiplication latency when $m = n = 12288$ as shown in Figure 9. It can be noticed that the additional search parameter g allows a fine-grained search space of compression ratio that is not available by q alone. Across all available compression ratios in Figure 9, latency is a function of

Table 2: Latency of the first FFN layer on OPT-175B model with various precision and corresponding kernel selections, while $m = 12288$. OPTQ kernel performs the dequantization process followed by GEMM. The latency measurements are taken on an A100 80GB GPU.

Kernel	Precision for Data Type			Latency (ms)
	Input ($1 \times m$)	Weight ($m \times 4m$)	Output ($1 \times 4m$)	
cuBLAS	FP32	FP32	FP32	1.4015
cuBLAS	FP16	FP16	FP16	0.7256
cuBLAS	INT8	INT8	INT32	0.6345
OPTQ [18]	FP16	INT3	FP16	0.3599
OPTQ [18]	FP32	INT3	FP32	0.3047
LUT-GEMM	FP16	BCQ8, INT8	FP16	0.4620
LUT-GEMM	FP16	BCQ3, INT3	FP16	0.1956

compression ratio. For instance, if two different pairs (q_1, g_1) and (q_2, g_2) exhibit a similar memory footprint, then we can expect similar latency by LUT-GEMM.

4 EXPERIMENTAL RESULTS

In this section, we present the experimental results obtained by utilizing LUT-GEMM across various levels of complexity, ranging from a single-layer experimental setup (excluding group size) to the complete model level. Initially, we examine the influence of LUT-GEMM on a specific layer, disregarding group size. Subsequently, we compare tensor parallelism with LUT-GEMM, followed by an investigation into the impact of group size. Finally, we analyze the end-to-end latency of OPT models [59] to determine the overall effect of LUT-GEMM on performance.

4.1 Simple Comparisons with Various Kernels

Table 2 presents the latency measurements for the first layer in the Feedforward Neural Network (FFN) on the OPT-175B model [59]. The results are obtained with various input and weight quantization methods, including FP-FP (baseline), INT-INT, FP-INT, and FP-BCQ. Kernels selected for the measurements include cuBLAS (for FP-FP or INT-INT), OPTQ[18] (for FP-INT), or LUT-GEMM (for FP-INT or FP-BCQ). Note that OPTQ kernel includes the dequantization process, followed by GEMM, whereas LUT-GEMM accepts row-wise quantized weights directly, without requiring dequantization. We can observe that the latency of the INT8-INT8 (with cuBLAS) implementation only shows marginal latency improvement over FP-FP since cuBLAS is not well-optimized for single batch operations. While OPTQ kernel achieves lower latency compared to the INT8-INT8 quantization method, it is slower than LUT-GEMM due to the overhead of dequantization. Thus, the proposed LUT-GEMM kernel, which supports both BCQ and INT quantization in a single kernel, achieves the lowest latency among the kernels considered.

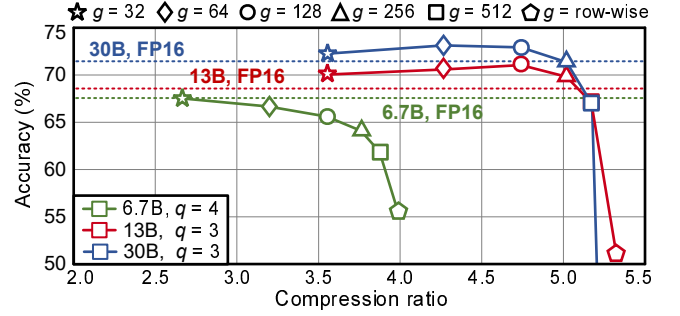


Figure 10: Accuracy and compression ratio with the various combinations of quantization bits (q) and group size (g). Three pre-trained OPT models are quantized (by post-training quantization method) and then evaluated on the LAMBADA dataset.

4.2 Comparison with FP16 Tensor Parallelism

Table 3 summarizes the profiling results of matrix multiplications performed by using cuBLAS (with tensor parallelism) or LUT-GEMM (with one GPU). GPU power and other metrics are collected by using *nvidia-smi* utility [1, 49]. Again, an $(m \times m)$ matrix is multiplied by an $(m \times 1)$ matrix, where we set m to be 8192 and 12288. This operation is particularly relevant to our investigation of GPT-3 175B, where the hidden size is 12288. We include the case of $q = 2$ for LUT-GEMM as 2-bit quantization for the Transformer is reported to be feasible by quantization-aware training along with BCQ format [12]. We notice that tensor parallelism with additional GPUs in cuBLAS brings about a significant decrease in GPU utilization, memory utilization, and computation latency ratios. As evidenced by the increase in the latency ratio of communication, such reductions in utilization indicate that some GPUs can be temporarily idle until all GPUs are synchronized. Accordingly, the amount of speed-up that can be obtained by tensor parallelism is a lot smaller than the number of GPUs. As a result, cuBLAS with more GPUs causes increased energy consumption for matrix multiplications. On the other hand, LUT-GEMM (with one GPU) can offer high speed-up (that cannot be achieved by tensor parallelism) while retaining high GPU/memory utilization. Combining low latency and a reduced number of GPUs, thus, LUT-GEMM substantially saves energy consumption for matrix multiplications. For example, when $m = 12288$, LUT-GEMM (with $q = 2$ and only one GPU) achieves $4.8\times$ energy reduction and $6.0\times$ speed-up compared to cuBLAS.

4.3 Exploration of Compression Ratio

To study the capability of group-wise BCQ to enlarge search space for compression, we conduct experiments on three pre-trained OPT models [59], which are publicly available². Specifically, we apply post-training quantization (with an iterative solver introduced in [54]) to pre-trained OPT models while g and q vary. Then, each quantized model is evaluated on the LAMBADA [40] dataset to

²<https://huggingface.co/facebook/opt-30b>

Table 3: Profiling results of matrix multiplications (with an $(m \times m)$ matrix and an $(m \times 1)$ matrix). For LUT-GEMM, $g = m$ and q is 2 or 4.

Type	GPUs	m	Comm. Ratio (%)	Speed Up	GPU Util. (%)	Memory Util. (%)	Avg. Power (W/GPU)	TotalEnergy (mJ)	Norm. Energy
cuBLAS	1	8192	0.00	1.00	90.97	46.77	248.27	47.50	1.00
cuBLAS	2	8192	23.73	1.30	69.84	30.42	203.91	59.98	1.26
cuBLAS	4	8192	33.42	1.24	48.60	14.46	142.57	88.20	1.86
cuBLAS	8	8192	44.84	0.96	34.26	5.61	86.80	138.34	2.91
LUT-GEMM ($q = 2$)	1	8192	0.00	4.41	73.96	25.75	179.72	7.81	0.16
LUT-GEMM ($q = 4$)	1	8192	0.00	3.15	81.97	36.84	234.09	14.21	0.30
cuBLAS	1	12288	0.00	1.00	95.98	39.61	228.74	118.46	1.00
cuBLAS	2	12288	11.58	1.60	84.43	31.62	216.61	137.91	1.16
cuBLAS	4	12288	24.13	2.18	66.19	21.63	178.19	165.80	1.40
cuBLAS	8	12288	38.58	2.01	42.57	9.93	124.82	252.99	2.14
LUT-GEMM ($q = 2$)	1	12288	0.00	6.04	83.92	29.89	289.11	24.34	0.21
LUT-GEMM ($q = 4$)	1	12288	0.00	4.32	89.98	42.78	328.57	38.66	0.33

find the relationship between compression ratio and accuracy. Figure 10 shows accuracy and compression ratio³ when we try various q values and g values. From Figure 10, we observe that compared to the conventional row-wise quantization, group-wise BCQ offers new optimal configurations (see Figure 11 in Appendix for our extensive results). Thus, to achieve the best compression ratio (or minimum accuracy degradation), it is necessary to explore different q and g values simultaneously for a given target. Note that for OPT-13B and OPT-30B, as we discussed the limits of row-wise quantization for large-scale LMs, a small g value is critical to achieving low accuracy degradation (while latency is not heavily affected by a small g). All in all, the effects of q and g on accuracy differ with each model such that q and g are hyper-parameters to be optimized.

4.4 End-to-end latency

Now, we evaluate the end-to-end latency of inference with a single batch size, considering various OPT models with quantized weights while maintaining full precision activations. Table 4 illustrates the end-to-end latency per token and perplexity when weights are uniformly quantized using the round-to-nearest (RTN) method. Note that the latency measurements are conducted within the FasterTransformer framework. We utilize different numbers of GPUs to access the potential speed-up gains achievable through model parallelism. From our observations in Table 4, we can conclude the following: 1) Reducing the group size (g) effectively decreases perplexity, even when employing a simple RTN quantization scheme, at the cost of a marginal increase in latency, 2) Increasing the number of GPUs (and, consequently, parallelism) does not significantly reduce latency due to various overheads such as GPU-to-GPU communication cost, as described in Figure 4. It is worth mentioning that, in the case of LUT-GEMM, where matrix multiplications are accelerated, relative GPU-to-GPU communication overheads become more pronounced compared to cuBLAS. As a result, model parallelism appears to be less effective for LUT-GEMM. In other words, for high-performance matrix multiplication engines, communication overheads become more prominent.

³Calculated as FP16 model size divided by each quantized model size.

In the case of the OPT-30B model, end-to-end inference with FP16 weights can be executed on a single GPU. However, for the OPT-66B model with FP16 weights, since the model size exceeds the memory capacity of a single GPU (80GB for A100), model parallelism techniques are mandated. Yet, when the weights of the OPT-66B model are quantized to 3 or 4 bits, as demonstrated to be a viable solution in [18], inference can be accommodated on a single GPU. Assuming 3-bit quantization and the implementation of LUT-GEMM with $g=32$, a speed-up of 2.43 \times for OPT-30B (using one GPU) and 2.25 \times for OPT-66B (using two GPUs) is attainable. Note that our demonstration of LUT-GEMM’s performance in Table 4 relies on a basic post-training quantization, while more advanced quantization methods for LLMs are available. For instance, when fine-tuning is performed subsequent to the construction of a pre-trained model, as exemplified in ChatGPT [39], more efficient quantization techniques such as AlphaTuning [29] can enable even 2-bit quantization. The utility of LUT-GEMM is further enhanced when combined with advanced quantization methods to reduce the number of quantization bits. Additional evaluation results can be found in Appendix A.1.

5 ACCELERATING QUANTIZED OPT-175B

Table 5 provides a comparison of the end-to-end latency for generating a token in OPT-175B, a representative large-scale LM, using the FasterTransformer framework. We evaluate three different implementations: 1) the original FP16 cuBLAS, 2) dequantization (from 3-bit) integrated with FP16 cuBLAS (using the library in OPTQ [18]), and 3) LUT-GEMM (assuming uniform quantization). By concentrating only on the four specific matrix multiplications previously discussed, LUT-GEMM demonstrate its ability to decrease the number of GPUs needed for running inference, while concurrently reducing latency as q diminishes or as the number of GPUs rises. For OPT-175B with FP16, a minimum of 8 GPUs is necessary for executing inference. However, upon applying the BCQ format for quantization, LUT-GEMM is able to perform inference using just a single GPU, while maintaining a comparable overall latency. It should be noted that, when comparing identical 3-bit (weight-only and row-wise) quantization scenarios, the latency for token generation using LUT-GEMM is 2.1 \times lower than that of the

Table 4: Comparison of perplexity and end-to-end latency per token for OPT models with cuBLAS and LUT-GEMM implementations with round-to-nearest (RTN) uniform quantization method and model parallelism on multiple GPUs.

Model	Bits	g	Quantization method	Perplexity			Kernel	Latency (ms)		
				Wiki2	PTB	LAMBADA		1-GPU	2-GPU	4-GPU
30B	16	-	FP16	9.56	11.84	15.84	cuBLAS	40.5	23.5	14.7
	4	32	Uniform (RTN)	9.71	12.02	16.16	LUT-GEMM	18.5	14.3	11.9
	4	64	Uniform (RTN)	9.88	12.05	16.17	LUT-GEMM	17.8	13.9	11.8
	3	32	Uniform (RTN)	10.78	13.89	19.21	LUT-GEMM	16.7	13.3	11.6
	3	64	Uniform (RTN)	14.61	24.63	31.13	LUT-GEMM	15.7	12.6	11.2
66B	16	-	FP16	9.34	11.36	15.47	cuBLAS	OOM	48.4	28.3
	4	32	Uniform (RTN)	9.54	11.55	15.83	LUT-GEMM	33.5	23.5	18.5
	4	64	Uniform (RTN)	9.54	11.63	15.91	LUT-GEMM	31.9	23.2	17.8
	3	32	Uniform (RTN)	18.82	35.76	42.16	LUT-GEMM	30.5	21.5	16.9
	3	64	Uniform (RTN)	51.15	130.54	130.19	LUT-GEMM	27.5	20.9	16.0

Table 5: End-to-end latency per token for OPT-175B model. The latency is measured on A100 80GB. Weights are uniformly quantized.

GPUs	Latency per token (ms)					
	Baseline	DQ(OPTQ)*		LUT-GEMM		
	FP16	3-bit	1-bit	2-bit	3-bit	4-bit
1	OOM	106.5	30.4	40.1	51.6	OOM
2	OOM	N/A	25.2	30.1	35.8	41.2
4	OOM	N/A	20.3	23.8	27.2	30.1
8	42.4	N/A	20.1	22.4	24.2	25.8

* Dequantization (from weight-only row-wise 3-bit) integrated with FP16 cuBLAS on a single GPU, as replicated using the methods and library presented in OPTQ [18].

Table 6: Perplexity of OPT-175B quantized using OPTQ and end-to-end latency per token by LUT-GEMM for various q and g configurations. g of ‘-’ indicates row-wise quantization.

Kernel	q	g	PPL*	Model size(GB) (Comp. Ratio)	Latency(ms)
cuBLAS	16	-	8.34	347.9 ($\times 1.00$)	42.4 (8-GPU)
	3	-	8.68	65.3 ($\times 5.33$)	51.6 (1-GPU)
LUT-GEMM	2	32	8.94	54.4 ($\times 6.40$)	55.2 (1-GPU)
	2	64	9.18	48.9 ($\times 7.11$)	47.5 (1-GPU)
	2	128	9.58	46.2 ($\times 7.53$)	46.5 (1-GPU)

* PPL numbers are extracted from the OPTQ reference [18].

OPTQ library. This significant reduction in latency can be primarily attributed to LUT-GEMM’s ability to directly accept quantized weights, thereby eliminating the need for dequantization.

Let us demonstrate that the flexible features of LUT-GEMM (attributable to the extended BCQ format) can accelerate existing uniform quantization methods. Table 6 shows the perplexity of OPT-175B for various q and g configurations, as obtained using the OPT-Q method. The table also displays the corresponding latency (per generated token) achieved by LUT-GEMM (excluding FP16). The results clearly indicate that LUT-GEMM provides lower latency as q decreases, although an excessively small g may have a marginal

adverse impact on latency. All in all, by integrating LUT-GEMM and OPTQ at the expense of an acceptable increase in perplexity, it is possible to reduce the number of GPUs required for running OPT-175B inference from eight GPUs to a single GPU while maintaining high performance. It is crucial to note that such an improvement in performance cannot be achieved when dequantization is included.

6 CONTEXT PROCESSING USING QUANTIZED WEIGHTS

As discussed, generative LM inference consists of two stages: summarization, using input context, and generation, as shown in Figure 3. These stages require different batch sizes. Summarization allows parallel processing of multiple tokens, while generation, due to its autoregressive nature, is a single-batch operation. Thus, generative LM inference balances compute-bound (high parallelism for context processing) and memory-bound (low parallelism for generation). Our proposed inference strategy involves storing quantized weights using (extended) BCQ. These weights are then: 1) dequantized to perform full-precision cuBLAS matrix multiplications during the context processing stage, and 2) utilized as inputs for LUT-GEMM during the generation stage. Note that weight quantization is essential for efficient memory usage, even during context processing. Furthermore, due to the high weight reuse ratio, the dequantization latency for context processing is relatively low compared to the generation stage. Consequently, LUT-GEMM becomes a desirable approach for the generation stage, which often dominates the overall inference latency as more tokens need to be generated (a common requirement for generative LMs).

7 CONCLUSION

Generative language models are attracting attention due to their generation capability on various complicated tasks. The inference speed, however, is a serious concern not only because of parameter size increase but also because of autoregressive operations associated with single-batch operation. To address such concerns, we proposed a new group-wise binary-coding quantization format and a dedicated matrix multiplication kernel LUT-GEMM. LUT-GEMM mitigates the need for tensor parallelism, which is typically

necessary when a model is too big to fit within a single GPU’s memory. Combining low latency and a reduced number of GPUs, LUT-GEMM enables significantly reduced energy consumption.

REFERENCES

- [1] Ghazanfar Ali, Sridutt Bhalachandra, Nicholas Wright, Alan Sill, and Yong Chen. 2020. Evaluation of power controls and counters on general-purpose Graphics Processing Units (GPUs). (2020).
- [2] Ammar Ahmad Awan, Ching-Hsiang Chu, Hari Subramoni, and Dhabaleswar K Panda. 2018. Optimized broadcast for deep learning workloads on dense-GPU InfiniBand clusters: MPI or NCCL?. In *Proceedings of the 25th European MPI Users’ Group Meeting*. 1–9.
- [3] Alexei Baevski, Yuhao Zhou, Abdelrahman Mohamed, and Michael Auli. 2020. wav2vec 2.0: A framework for self-supervised learning of speech representations. *Advances in neural information processing systems* 33 (2020), 12449–12460.
- [4] Nathan Bell and Michael Garland. 2008. *Efficient sparse matrix-vector multiplication on CUDA*. Technical Report.
- [5] Aishwarya Bhandare, Vamsi Sripathi, Deepthi Karkada, Vivek Menon, Sun Choi, Kushal Datta, and Vikram Salatore. 2019. Efficient 8-Bit Quantization of Transformer Neural Machine Language Translation Model. *arXiv:1906.00532* (2019).
- [6] Tom Brown, Benjamin Mann, Nick Ryder, Melanie Subbiah, Jared D Kaplan, Prafulla Dhariwal, Arvind Neelakantan, Pranav Shyam, Girish Sastry, Amanda Askell, et al. 2020. Language models are few-shot learners. *Advances in neural information processing systems* 33 (2020), 1877–1901.
- [7] Patrick Chen, Si Si, Yang Li, Ciprian Chelba, and Cho-Jui Hsieh. 2018. GroupReduce: Block-wise low-rank approximation for neural language model shrinking. In *Advances in Neural Information Processing Systems*.
- [8] Ting Chen, Simon Kornblith, Mohammad Norouzi, and Geoffrey Hinton. 2020. A simple framework for contrastive learning of visual representations. In *International conference on machine learning*. PMLR, 1597–1607.
- [9] Weihao Chen, Peisong Wang, and Jian Cheng. 2021. Towards Mixed-Precision Quantization of Neural Networks via Constrained Optimization. In *Proceedings of the IEEE/CVF International Conference on Computer Vision*. 5350–5359.
- [10] Yoojin Choi, Mostafa El-Khamy, and Jungwon Lee. 2017. Towards the limit of network quantization. In *International Conference on Learning Representations (ICLR)*.
- [11] Aakanksha Chowdhery, Sharan Narang, Jacob Devlin, Maarten Bosma, Gaurav Mishra, Adam Roberts, Paul Barham, Hyung Won Chung, Charles Sutton, Sebastian Gehrmann, Parker Schuh, Kensen Shi, Sasha Tsvyashchenko, Joshua Maynez, Abhishek Rao, Parker Barnes, Yi Tay, Noam Shazeer, Vinodkumar Prabhakaran, Emily Reif, Nan Du, Ben Hutchinson, Reiner Pope, James Bradbury, Jacob Austin, Michael Isard, Guy Gur-Ari, Pengcheng Yin, Toju Duke, Anselm Levskaya, Sanjay Ghemawat, Sunipa Dev, Henryk Michalewski, Xavier Garcia, Vedant Misra, Kevin Robinson, Liam Fedus, Denny Zhou, Daphne Ipollito, David Luan, Hyeontaek Lim, Barret Zoph, Alexander Spiridonov, Ryan Sepassi, David Dohan, Shivani Agrawal, Mark Omernick, Andrew M. Dai, Thanumalayan Sankaranarayanan Pillai, Marie Pellat, Aitor Lewkowycz, Erica Moreira, Rewon Child, Oleksandr Polozov, Katherine Lee, Zongwei Zhou, Xuezhi Wang, Brennan Saeta, Mark Diaz, Orhan Firat, Michele Catasta, Jason Wei, Kathy Meier-Hellstern, Douglas Eck, Jeff Dean, Slav Petrov, and Noah Fiedel. 2022. PaLM: Scaling Language Modeling with Pathways. <https://doi.org/10.48550/ARXIV.2204.02311>
- [12] Insoo Chung, Byeongwook Kim, Yoonjung Choi, Se Jung Kwon, Yongkweon Jeon, Baeseong Park, Sangha Kim, and Dongsoo Lee. 2020. Extremely Low Bit Transformer Quantization for On-Device Neural Machine Translation. In *Findings of the Association for Computational Linguistics: EMNLP 2020*. 4812–4826.
- [13] R.L. de Queiroz and P.A. Stein. 2004. LUT filters for quantized processing of signals. *IEEE Transactions on Signal Processing* 52, 3 (2004), 687–693.
- [14] Tim Dettmers, Mike Lewis, Younes Belkada, and Luke Zettlemoyer. 2022. LLM.int8(): 8-bit Matrix Multiplication for Transformers at Scale. *arXiv preprint arXiv:2208.07339* (2022).
- [15] Jacob Devlin, Ming-Wei Chang, Kenton Lee, and Kristina Toutanova. 2019. BERT: Pre-training of Deep Bidirectional Transformers for Language Understanding. In *Proceedings of the 2019 Conference of the North American Chapter of the Association for Computational Linguistics: Human Language Technologies, Volume 1 (Long and Short Papers)*. 4171–4186.
- [16] Ali Edalati, Marzieh Tahaei, Ahmad Rashid, Vahid Partovi Nia, James J. Clark, and Mehdi Rezagholizadeh. 2021. Kronecker Decomposition for GPT Compression. *arXiv:2110.08152* [cs.CL]
- [17] Elias Frantar and Dan Alistarh. 2023. SparseGPT: Massive Language Models Can Be Accurately Pruned in One-Shot. *arXiv:2301.00774* [cs.LG]
- [18] Elias Frantar, Saleh Ashkboos, Torsten Hoefler, and Dan Alistarh. 2022. GPTQ: Accurate Post-Training Quantization for Generative Pre-trained Transformers. <https://doi.org/10.48550/ARXIV.2210.17323>
- [19] Trevor Gale, Erich Elsen, and Sara Hooker. 2019. The state of sparsity in deep neural networks. *arXiv preprint arXiv:1902.09574* (2019).
- [20] Yiwen Guo, Anbang Yao, Hao Zhao, and Yurong Chen. 2017. Network sketching: exploiting binary structure in deep CNNs. In *IEEE Conference on Computer Vision and Pattern Recognition (CVPR)*. 4040–4048.
- [21] Song Han, Huizi Mao, and William J. Dally. 2016. DEEP COMPRESSION: COMPRESSING DEEP NEURAL NETWORKS WITH PRUNING, TRAINED QUANTIZATION AND HUFFMAN CODING. In *International Conference on Learning Representations (ICLR)*.
- [22] Geoffrey Hinton, Oriol Vinyals, and Jeff Dean. 2015. Distilling the knowledge in a neural network. In *NIPS Deep Learning and Representation Learning Workshop*.
- [23] Jordan Hoffmann, Sebastian Borgeaud, Arthur Mensch, Elena Buchatskaya, Trevor Cai, Eliza Rutherford, Diego de Las Casas, Lisa Anne Hendricks, Johannes Welbl, Aidan Clark, et al. 2022. Training compute-optimal large language models. *arXiv preprint arXiv:2203.15556* (2022).
- [24] Benoit Jacob, Skirmantas Kligys, Bo Chen, Menglong Zhu, Matthew Tang, Andrew Howard, Hartwig Adam, and Dmitry Kalenichenko. 2018. Quantization and training of neural networks for efficient integer-arithmetic-only inference. In *Proceedings of the IEEE Conference on Computer Vision and Pattern Recognition*. 2704–2713.
- [25] Yongkweon Jeon, Baeseong Park, Se Jung Kwon, Byeongwook Kim, Jeongin Yun, and Dongsoo Lee. 2020. Biggemm: matrix multiplication with lookup table for binary-coding-based quantized dnn. In *SC20: International Conference for High Performance Computing, Networking, Storage and Analysis*. IEEE, 1–14.
- [26] Jared Kaplan, Sam McCandlish, Tom Henighan, Tom B. Brown, Benjamin Chess, Rewon Child, Scott Gray, Alec Radford, Jeffrey Wu, and Dario Amodei. 2020. Scaling Laws for Neural Language Models. *arXiv:2001.08361* (2020).
- [27] Boseop Kim, Hyoungseok Kim, Sang-Woo Lee, Gichang Lee, Donghyun Kwak, Jeon Dong Hyeon, Sunghyun Park, Sungju Kim, Seonhoon Kim, Dongpil Seo, et al. 2021. What Changes Can Large-scale Language Models Bring? Intensive Study on HyperCLOVA: Billions-scale Korean Generative Pretrained Transformers. In *Proceedings of the 2021 Conference on Empirical Methods in Natural Language Processing*. 3405–3424.
- [28] Sehoon Kim, Amir Gholami, Zhewei Yao, Michael W Mahoney, and Kurt Keutzer. 2021. I-bert: Integer-only bert quantization. In *International conference on machine learning*. PMLR, 5506–5518.
- [29] Se Jung Kwon, Jeonghoon Kim, Jeongin Bae, Kang Min Yoo, Jin-Hwa Kim, Baeseong Park, Byeongwook Kim, Jung-Woo Ha, Nako Sung, and Dongsoo Lee. 2022. AlphaTuning: Quantization-Aware Parameter-Efficient Adaptation of Large-Scale Pre-Trained Language Models. In *Findings of EMNLP 2022*.
- [30] Ang Li, Shuaiwen Leon Song, Jieyang Chen, Jiajia Li, Xu Liu, Nathan R Tallent, and Kevin J Barker. 2019. Evaluating modern gpu interconnect: Pcie, nvlink, nv-sli, nvswitch and gpudirect. *IEEE Transactions on Parallel and Distributed Systems* 31, 1 (2019), 94–110.
- [31] Darryl Lin, Sachin Talathi, and Sreekanth Annapureddy. 2016. Fixed point quantization of deep convolutional networks. In *International Conference on Machine Learning*. 2849–2858.
- [32] Stefano Markidis, Steven Wei Der Chien, Erwin Laure, Ivy Bo Peng, and Jeffrey S Vetter. 2018. Nvidia tensor core programmability, performance & precision. In *2018 IEEE international parallel and distributed processing symposium workshops (IPDPSW)*. IEEE, 522–531.
- [33] Mark D. McDonnell. 2018. Training wide residual networks for deployment using a single bit for each weight. In *International Conference on Learning Representations (ICLR)*.
- [34] Pramod Kumar Meher. 2010. LUT Optimization for Memory-Based Computation. *IEEE Transactions on Circuits and Systems II: Express Briefs* 57, 4 (2010), 285–289.
- [35] Szymon Migacz. 2017. 8-bit Inference with TensorRT. In *NVIDIA GPU Technology conference*.
- [36] Tara N. Sainath, Brian Kingsbury, Vikas Sindhwani, Ebru Arisoy, and Bhuvana Ramabhadran. 2013. Low-rank matrix factorization for deep neural network training with high-dimensional output targets. In *ICASSP*. 6655–6659.
- [37] Markus Nagel, Rana Ali Amjad, Mart van Baalen, Christos Louizos, and Tijmen Blankevoort. 2017. Up or Down? Adaptive Rounding for Post-Training Quantization. In *International Conference on Machine Learning (ICML)*. 7696–7705.
- [38] Deepak Narayanan, Mohammad Shoeybi, Jared Casper, Patrick LeGresley, Mostafa Patwary, Vijay Korthikanti, Dmitri Vainbrand, Prithvi Kashinkunti, Julie Bernauer, Bryan Catanzaro, et al. 2021. Efficient large-scale language model training on GPU clusters using megatron-LM. In *Proceedings of the International Conference for High Performance Computing, Networking, Storage and Analysis*. 1–15.
- [39] openAI. 2023. GPT-4 Technical Report. *arXiv:2303.08774* (2023).
- [40] Denis Paperno, Germán Kruszewski, Angeliki Lazaridou, Quan Ngoc Pham, Raffaella Bernardi, Sandro Pezzelle, Marco Baroni, Gemma Boleda, and Raquel Fernández. 2016. *The LAMBADA dataset*. <https://doi.org/10.5281/zenodo.2630551>
- [41] Antonio Polino, Razvan Pascanu, and Dan Alistarh. 2018. Model compression via distillation and quantization. In *International Conference on Learning Representations (ICLR)*.
- [42] Jan M. Rabaey, Anantha Chandrakasan, and Borivoje Nikolic. 2004. *Digital integrated circuits- A design perspective* (2ed ed.). Prentice Hall.

- [43] Jack W. Rae, Sebastian Borgeaud, Trevor Cai, Katie Millican, Jordan Hoffmann, Francis Song, John Aslanides, Sarah Henderson, Roman Ring, Susannah Young, Eliza Rutherford, Tom Hennigan, Jacob Menick, Albin Cassirer, Richard Powell, George van den Driessche, Lisa Anne Hendricks, Maribeth Rauh, Po-Sen Huang, Amelia Glaese, Johannes Welbl, Sumanth Dathathri, Saffron Huang, Jonathan Uesato, John Mellor, Irina Higgins, Antonia Creswell, Nat McAleese, Amy Wu, Erich Elsen, Siddhant Jayakumar, Elena Buchatskaya, David Budden, Esme Sutherland, Karen Simonyan, Michela Paganini, Laurent Sifre, Lena Martens, Xiang Lorraine Li, Adhiguna Kuncoro, Aida Nematzadeh, Elena Gribovskaya, Domenic Donato, Angeliki Lazaridou, Arthur Mensch, Jean-Baptiste Lespiau, Maria Tsimpoukelli, Nikolai Grigorev, Doug Fritz, Thibault Sottiaux, Mantas Pajarskas, Toby Pohlen, Zhitao Gong, Daniel Toyama, Cyprien de Masson d’Autume, Yujia Li, Tayfun Terzi, Vladimir Mikulik, Igor Babuschkin, Aidan Clark, Diego de Las Casas, Aurelia Guy, Chris Jones, James Bradbury, Matthew Johnson, Blake Hechtman, Laura Weidinger, Iason Gabriel, William Isaac, Ed Lockhart, Simon Osindero, Laura Rimell, Chris Dyer, Oriol Vinyals, Kareem Ayoub, Jeff Stanway, Lorraine Bennett, Demis Hassabis, Koray Kavukcuoglu, and Geoffrey Irving. 2021. Scaling Language Models: Methods, Analysis & Insights from Training Gopher. *arXiv:2112.11446* (2021).
- [44] Samyam Rajbhandari, Olatunji Ruwase, Jeff Rasley, Shaden Smith, and Yuxiong He. 2021. Zero-infinity: Breaking the gpu memory wall for extreme scale deep learning. In *Proceedings of the International Conference for High Performance Computing, Networking, Storage and Analysis*. 1–14.
- [45] Mohammad Rastegari, Vicente Ordonez, Joseph Redmon, and Ali Farhadi. 2016. XNOR-Net: ImageNet Classification Using Binary Convolutional Neural Networks. In *ECCV*.
- [46] Sudip Roy, Jeff Dean, Sanjay Ghemawat, Ryan Sepassi, Hyeontaek Lim, Michael Isard, Paul Barham, Yonghui Wu, Laurent Shafey, Aakanksha Chowdhery, et al. 2022. Pathways: Asynchronous Distributed Dataflow for ML. *Proceedings of Machine Learning and Systems* 4 (2022).
- [47] Mohammad Shoeybi, Mostofa Patwary, Raul Puri, Patrick LeGresley, Jared Casper, and Bryan Catanzaro. 2019. Megatron-lm: Training multi-billion parameter language models using model parallelism. *arXiv preprint arXiv:1909.08053* (2019).
- [48] Shaden Smith, Mostofa Patwary, Brandon Norick, Patrick LeGresley, Samyam Rajbhandari, Jared Casper, Zhun Liu, Shrimai Prabhumoye, George Zerveas, Vijay Korthikanti, et al. 2022. Using DeepSpeed and Megatron to Train Megatron-Turing NLG 530B, A Large-Scale Generative Language Model. *arXiv preprint arXiv:2201.11990* (2022).
- [49] Devesh Tiwari, Saurabh Gupta, George Gallarno, Jim Rogers, and Don Maxwell. 2015. Reliability lessons learned from gpu experience with the titan supercomputer at oak ridge leadership computing facility. In *Proceedings of the International Conference for High Performance Computing, Networking, Storage and Analysis*. 1–12.
- [50] Ashish Vaswani, Noam Shazeer, Niki Parmar, Jakob Uszkoreit, Llion Jones, Aidan N Gomez, Łukasz Kaiser, and Illia Polosukhin. 2017. Attention is all you need. *Advances in neural information processing systems* 30 (2017).
- [51] Bichen Wu, Yanghan Wang, Peizhao Zhang, Yuandong Tian, Peter Vajda, and Kurt Keutzer. 2018. Mixed Precision Quantization of ConvNets via Differentiable Neural Architecture Search. *arXiv:1812.00090* (2018).
- [52] Shuang Wu, Guoqi Li, Feng Chen, and Luping Shi. 2018. Training and Inference with Integers in Deep Neural Networks. In *International Conference on Learning Representations (ICLR)*.
- [53] Guangxuan Xiao, Ji Lin, Mickael Seznec, Julien Demouth, and Song Han. 2022. SmoothQuant: Accurate and Efficient Post-Training Quantization for Large Language Models. <https://doi.org/10.48550/ARXIV.2211.10438>
- [54] Chen Xu, Jianqiang Yao, Zhouchen Lin, Wenwu Ou, Yuanbin Cao, Zhirong Wang, and Hongbin Zha. 2018. Alternating Multi-bit Quantization for Recurrent Neural Networks. In *International Conference on Learning Representations (ICLR)*.
- [55] Shiyu Xu, Qi Wang, Xingbo Wang, Shihang Wang, and Terry Tao Ye. 2021. Multiplication Through a Single Look-Up-Table (LUT) in CNN Inference Computation. *IEEE Transactions on Computer-Aided Design of Integrated Circuits and Systems* (2021), 1–1.
- [56] Zhewei Yao, Reza Yazdani Aminabadi, Minjia Zhang, Xiaoxia Wu, Conglong Li, and Yuxiong He. 2022. ZeroQuant: Efficient and Affordable Post-Training Quantization for Large-Scale Transformers. *arXiv preprint arXiv:2206.01861* (2022).
- [57] Jiecao Yu, Andrew Lukefahr, David Palframan, Ganesh Dasika, Reetuparna Das, and Scott Mahlke. 2017. Scalpel: Customizing DNN Pruning to the Underlying Hardware Parallelism. In *Proceedings of the 44th Annual International Symposium on Computer Architecture*. 548–560.
- [58] Aohan Zeng, Xiao Liu, Zhengxiao Du, Zihan Wang, Hanyu Lai, Ming Ding, Zhuoyi Yang, Yifan Xu, Wendi Zheng, Xiao Xia, Weng Lam Tam, Zixuan Ma, Yufei Xue, Jidong Zhai, Wenguang Chen, Peng Zhang, Yuxiao Dong, and Jie Tang. 2022. GLM-130B: An Open Bilingual Pre-trained Model. <https://doi.org/10.48550/ARXIV.2210.02414>
- [59] Susan Zhang, Stephen Roller, Naman Goyal, Mikel Artetxe, Moya Chen, Shuohui Chen, Christopher Dewan, Mona Diab, Xian Li, Xi Victoria Lin, Todor Mihaylov, Myle Ott, Sam Shleifer, Kurt Shuster, Daniel Simig, Punit Singh Koura, Anjali Sridhar, Tianlu Wang, and Luke Zettlemoyer. 2022. OPT: Open Pre-trained Transformer Language Models. *arXiv:2205.01068* (2022).
- [60] Ritchie Zhao, Yuwei Hu, Jordan Dotzel, Christopher De Sa, and Zhiru Zhang. 2019. Improving Neural Network Quantization without Retraining using Outlier Channel Splitting. In *International Conference on Machine Learning (ICML)*. 7543–7552.
- [61] Xuda Zhou, Zidong Du, Qi Guo, Shaoli Liu, Chengsi Liu, Chao Wang, Xuehai Zhou, Ling Li, Tianshi Chen, and Yunji Chen. 2018. Cambricon-S: Addressing Irregularity in Sparse Neural Networks through A Cooperative Software/Hardware Approach. In *2018 51st Annual IEEE/ACM International Symposium on Microarchitecture (MICRO)*. IEEE, 15–28.
- [62] Michael Zhu and Suyog Gupta. 2017. To prune, or not to prune: exploring the efficacy of pruning for model compression. *CoRR* abs/1710.01878 (2017).

A APPENDIX

A.1 Additional Evaluation Results

Table 7: Comparison between FP16 GEMM in cuBLAS and LUT-GEMM. An $(m \times n)$ matrix is multiplied by $(n \times 1)$ matrix as a single-batch operation. Row-wise scale factor assignment is assumed ($g = m$).

$m = n$	q	Memory (MB)		Latency (μ s)	
		FP16	LUT-GEMM (Reduction)	FP16	LUT-GEMM (Speed up)
4096	2		4.2 (x8.0)		20.2 (x3.4)
	3		6.3 (x5.3)		22.2 (x3.1)
	4	33.6	8.4 (x4.0)	68.8	24.3 (x2.8)
	5		10.5 (x3.2)		26.0 (x2.6)
7168	2		12.9 (x8.0)		35.9 (x4.6)
	3		19.3 (x5.3)		41.8 (x3.9)
	4	102.8	25.7 (x4.0)	165.2	47.1 (x3.5)
	5		32.1 (x3.2)		55.2 (x3.0)
12288	2		37.8 (x8.0)		84.2 (x6.0)
	3		56.6 (x5.3)		101.0 (x5.0)
	4	302.0	75.5 (x4.0)	508.2	117.7 (x4.3)
	5		94.4 (x3.2)		135.4 (x3.8)

For Table 4, we utilize OPTQ repository⁴ for the evaluation method without any modification.

Table 7 compares memory footprint and latency between conventional FP16 GEMM kernel in cuBLAS library and our proposed LUT-GEMM. For experiments, we multiply an $(m \times n)$ matrix (that can be quantized by q bits) and an $(n \times 1)$ matrix using a single Nvidia A100 40GB GPU with CUDA 11.3. We can observe that both the memory size and execution time required for cuBLAS and LUT-GEMM increase with larger m values (and LUT-GEMM, q values also contribute this increase). It is clear that the relative reduction of memory footprint and latency by LUT-GEMM increases when a larger weight matrix is employed. Such observation can be partly explained by the fact that kernel launch overhead appears as a performance bottleneck for small matrices (such as $m = 4096$). Thus, the merits of LUT-GEMM would be outstanding as larger-scale generative LMs are introduced.

Table 8 shows the accuracy of AlphaTuning with 2-bit quantization. We utilize a pre-trained OPT 1.3B and 2.7B model to be adapted via full fine-tuning or AlphaTuning [29] on GLUE-MNLI. For text classification tasks on MNLI, an LM head layer is added on top of OPT model with randomly initialized weights. We trained OPT models for 3 epochs, using a learning rate of 0.00001 for group sizes ranging from 32 to 256 and 0.00005 for group sizes above 1024. Additionally, we used a weight decay of 0.05 across all experiments. When initializing Alpha in AlphaTuning, we apply alternating quantization method [54].

Figure 11 and Figure 12 show supplementary results for language generation tasks using various number of quantization bit (q) values and group sizes (g).

Table 8: Accuracy achieved with 2-bit AlphaTuning on the MNLI dataset.

Model	Method	g	Acc. (%)	mm Acc. (%)
OPT-1.3B	Full fine-tune	-	87.5	87.4
		2048	85.0	84.9
	AlphaTuning	1024	85.1	85.1
		256	85.3	85.6
		128	85.7	86.2
		64	86.3	86.6
		32	86.5	87.1
OPT-2.7B	Full fine-tune	-	88.5	88.4
		1280	85.5	86.0
	AlphaTuning	256	86.8	87.7
		128	87.3	87.8
		64	87.4	87.9
		32	87.6	88.4

A.2 Mixed Precision using LUT-GEMM

It is well known that different layers of neural networks present different sensitivity to model compression [9, 21]. As such, mixed precision techniques for quantization are eligible for obtaining higher compression ratio practical techniques by assigning different quantization bits to layers while measuring accurate sensitivity of layers is complicated and computationally demanding [9, 51]. Note that since we introduce an additional parameter g (i.e., group size for scaling factors), LUT-GEMM can offer wider search space exploration for mixed precision compared to the conventional methods allowing the number of quantization bits as the only search parameter.

For experiments, we consider two sub-layers (multi-head attention and feed-forward networks) in Fig. 13 to be quantized by different quantization schemes with LUT-GEMM. In order to facilitate efficient exploration of search space for mixed precision, we set the following constraints: 1) all matrices of each sub-layer type (i.e., multi-head attention or feed-forward network) across all layers are quantized by the same (q, g) configuration, 2) q is selected to be one of $\{3, 4, 5\}$, and 3) g is selected to be one of $\{128, 256, 512, 2048\}$ that lead to less than 3% latency overhead compared to row-wise quantization as depicted in Fig. 8. Fig. 14 shows PPL degradation of GPT Neo 1.3B quantized by mixed precision (using two (q, g) configurations as described above). Notice that mixed precision combined with additional parameter g produces extensive trade-offs between PPL degradation and compression ratio.

⁴<https://github.com/IST-DASLab/gptq>

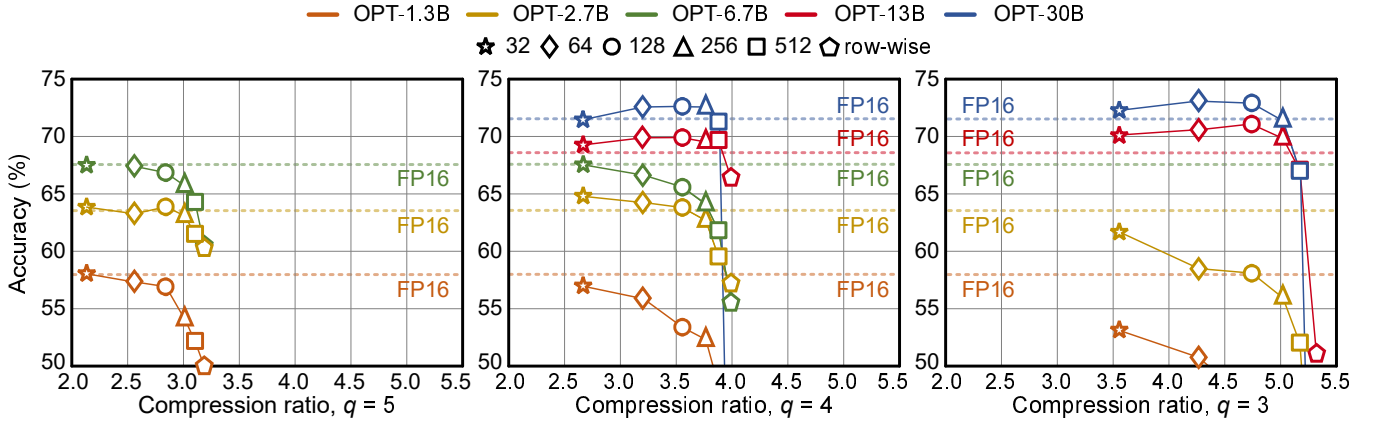


Figure 11: Accuracy and compression ratio of OPT models with the various number of quantization bits (q) and group size (g) on the LAMBADA dataset.

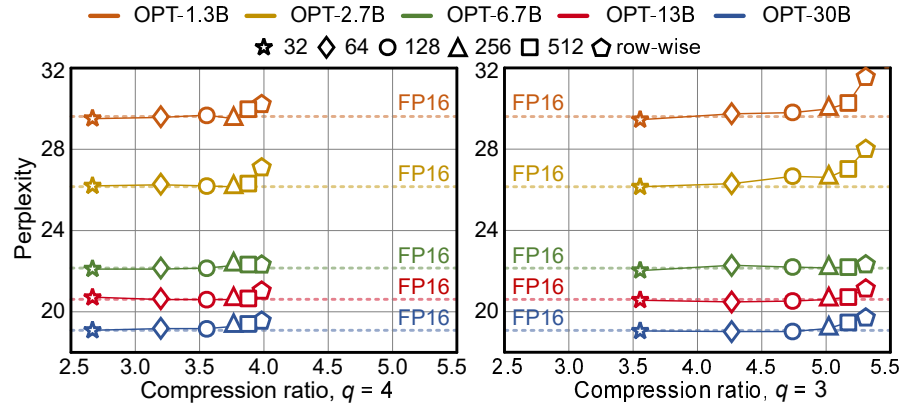


Figure 12: Perplexity and compression ratio with the various number of quantization bits (q) and group size (g) on the WikiText-2 dataset.

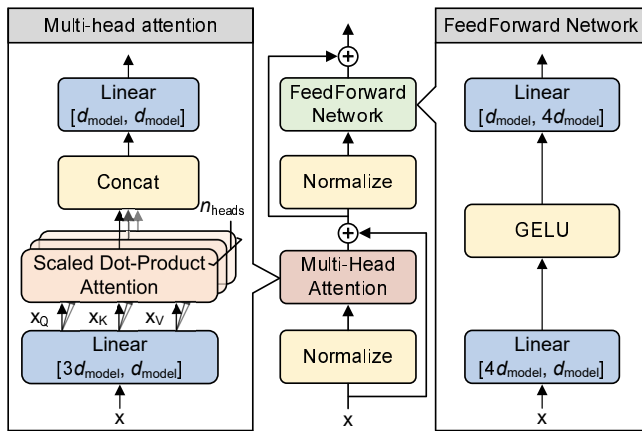


Figure 13: Transformer layer incorporating multi-head attention and feed-forward network performing 4 major matrix multiplications.

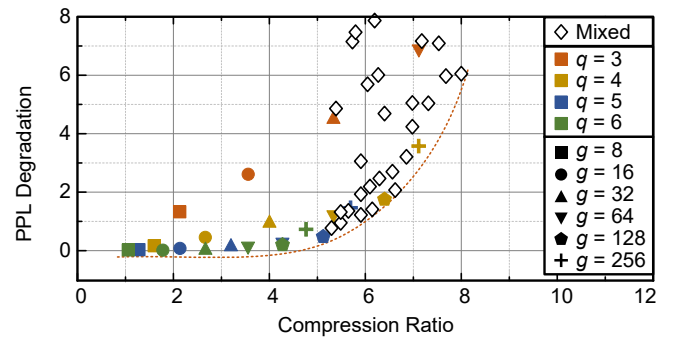


Figure 14: Mixed precision quantization results using GPT Neo 1.3B. All matrices of the same sub-layer type are quantized by the same (q, g) configuration. Available sets for exploring q and g are $\{3, 4, 5\}$ and $\{128, 256, 512, 2048\}$, respectively.

A.3 Inference Strategy for Context and Generation Process

Figure 15 shows inference strategy to support both context and generation process.

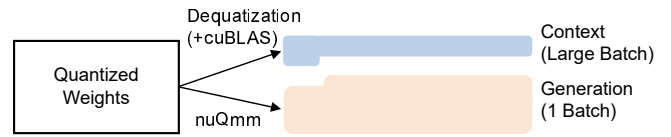


Figure 15: Our proposed strategy to support both context process and generation process using quantized weight with BCQ format.

This figure "acm-jdslogo.png" is available in "png" format from:

<http://arxiv.org/ps/2206.09557v3>

This figure "sample-franklin.png" is available in "png" format from:

<http://arxiv.org/ps/2206.09557v3>